



# 1 **Bipolar volcanic synchronization of abrupt climate change in** 2 **Greenland and Antarctic ice cores during the last glacial period**

3 Anders Svensson<sup>1</sup>, Dorthe Dahl-Jensen<sup>1</sup>, Jørgen Peder Steffensen<sup>1</sup>, Thomas Blunier<sup>1</sup>, Sune O.  
4 Rasmussen<sup>1</sup>, Bo M. Vinther<sup>1</sup>, Paul Vallelonga<sup>1</sup>, Emilie Capron<sup>1</sup>, Vasileios Gkinis<sup>1</sup>, Eliza Cook<sup>1</sup>, Helle  
5 Astrid Kjær<sup>1</sup>, Raimund Muscheler<sup>2</sup>, Sepp Kipfstuhl<sup>1,3</sup>, Frank Wilhelms<sup>3</sup>, Thomas F. Stocker<sup>4</sup>, Hubertus  
6 Fischer<sup>4</sup>, Florian Adolphi<sup>2,4</sup>, Tobias Erhardt<sup>4</sup>, Michael Sigl<sup>4</sup>, Amaelle Landais<sup>5</sup>, Frédéric Parrenin<sup>6</sup>,  
7 Christo Buizert<sup>7</sup>, Joseph R. McConnell<sup>8</sup>, Mirko Severi<sup>9</sup>, Robert Mulvaney<sup>10</sup> and Matthias Bigler<sup>4</sup>

8 <sup>1</sup>Physics of Ice, Climate and Earth, Niels Bohr Institute, University of Copenhagen, Copenhagen, Denmark

9 <sup>2</sup>Quaternary Sciences, Department of Geology, Lund University, Lund, Sweden

10 <sup>3</sup>Stiftung Alfred-Wegener-Institut für Polar- und Meeresforschung, Bremerhaven, Germany

11 <sup>4</sup>Climate and Environmental Physics, Physics Institute & Oeschger Centre for Climate Change Research, University of Bern,  
12 Bern, Switzerland.

13 <sup>5</sup>Laboratoire des Sciences du Climat et de l'Environnement, IPSL, UMR 8212, CEA-CNRS-UVSQ-UPS, Gif sur Yvette, France

14 <sup>6</sup>Université Grenoble Alpes, CNRS, IRD, IGE, Grenoble, France

15 <sup>7</sup>College of Earth, Ocean and Atmospheric Sciences, Oregon State University, Corvallis, OR, United States

16 <sup>8</sup>Desert Research Institute, Nevada System of Higher Education, Reno, NV, United States

17 <sup>9</sup>Department of Chemistry 'Ugo Schiff', University of Florence, Florence, Italy

18 <sup>10</sup>British Antarctic Survey, Cambridge, United Kingdom

19

## 20 **Abstract**

21 The last glacial period is characterized by a number of abrupt climate events that have been identified in both  
22 Greenland and Antarctic ice cores. The mechanisms governing this climate variability remain a puzzle that  
23 requires a precise synchronization of ice cores from the two Hemispheres to be resolved. Previously, Greenland  
24 and Antarctic ice cores have been synchronized primarily via their common records of gas concentrations or  
25 isotopes from the trapped air and via cosmogenic isotopes measured on the ice. In this work, we apply ice-core  
26 volcanic proxies and annual layer counting to identify large volcanic eruptions that have left a signature in both  
27 Greenland and Antarctica. Generally, no tephra is associated with those eruptions in the ice cores, so the source  
28 of the eruptions cannot be identified. Instead, we identify and match sequences of volcanic eruptions with  
29 bipolar distribution of sulfate, i.e. unique patterns of volcanic events separated by the same number of years at  
30 the two poles. Using this approach, we pinpoint 80 large bipolar volcanic eruptions throughout the second half  
31 of the last glacial period (12-60 ka before present). This improved ice-core synchronization is applied to  
32 determine the bipolar phasing of abrupt climate change events at decadal-scale precision. During abrupt  
33 transitions, we find more coherent Antarctic water isotopic signals ( $\delta^{18}\text{O}$  and deuterium excess) than was  
34 obtained from previous gas-based synchronizations, providing additional support for our volcanic framework.  
35 On average, the Antarctic bipolar seesaw climate response lags the midpoint of Greenland abrupt  $\delta^{18}\text{O}$   
36 transitions by  $122 \pm 24$  years. The time difference between Antarctic signals in deuterium excess and  $\delta^{18}\text{O}$ , which  
37 is less sensitive to synchronization errors, suggests an Antarctic  $\delta^{18}\text{O}$  lag of  $152 \pm 37$  years. These estimates are  
38 shorter than the 200 years suggested by earlier gas-based synchronizations. As before, we find variations in the



39 timing and duration between the response at different sites and for different events suggesting an interaction of  
40 oceanic and atmospheric teleconnection patterns as well as internal climate variability.

## 41 1. Introduction

42 Greenland and Antarctic ice cores provide high-resolution records of abrupt climate events occurring throughout  
43 the last glacial period (11.7-115 ka BP). In Greenland ice cores, Dansgaard-Oeschger (DO) events describe a series  
44 of characteristic climate events (Dansgaard et al., 1993; North Greenland Ice Core Project members, 2004) that  
45 involve warming transitions of up to 16.5 degrees (Kindler et al., 2014) occurring within decades (Erhardt et al.,  
46 2019). Each DO event consists of a relatively mild climatic period, referred to as a Greenland Interstadial (GI) that  
47 is followed by a cold climatic period, known as a Greenland Stadial (GS). The duration of GIs and GSs range from  
48 centuries to millennia. Detailed investigation of the stratigraphy of the 25 major DO events originally identified  
49 has revealed that some of the events are composed of several separate warming and cooling events, leading to  
50 a total of 31-33 abrupt warming events during the last glacial period depending on the definition employed  
51 (Rasmussen et al., 2014). Whereas the onset of a GI event is abrupt and occurs in less than a century, the cooling  
52 transitions from GI to GS are more gradual and typically occur over several centuries. DO events are believed to  
53 originate in the North Atlantic, but have a global climatic impact that is documented in a wide range of  
54 paleoclimate archives across the Northern Hemisphere (Voelker and workshop participants, 2002). In Antarctic  
55 ice cores, the corresponding Antarctic Isotopic Maxima (AIM) are characteristic warm events that are more  
56 gradual and of smaller amplitude than the Greenland events (EPICA community members, 2006). The AIMs are  
57 believed to be related to the DO events through the so-called bipolar seesaw mechanism (Bender et al., 1994;  
58 Stocker and Johnsen, 2003), but the detailed mechanism is a matter of debate (Landais et al., 2015; Pedro et al.,  
59 2018). Knowledge of the exact phasing of climate in the two Hemispheres is crucial for deciphering the driving  
60 mechanism of the abrupt climate variability of the last glacial period and the climatic teleconnection patterns  
61 that connect the two hemispheres.

62 Three different techniques have been applied to progressively improve the synchronization of Greenland and  
63 Antarctic ice cores: globally well-mixed atmospheric gases, in particular the methane concentration (Blunier et  
64 al., 1998; Buizert et al., 2015; Lemieux-Dudon et al., 2010) and the isotopic compositions of O<sub>2</sub>, δ<sup>18</sup>O<sub>atm</sub> (Bender  
65 et al., 1994; Capron et al., 2010), cosmogenic isotopes such as <sup>10</sup>Be and <sup>36</sup>Cl (Raisbeck et al., 2017; Steinhilber  
66 et al., 2012), and identification of large volcanic eruptions with bipolar sulfate deposition (Sigl et al., 2013; Svensson  
67 et al., 2013). A strength of the bipolar methane matching approach is that atmospheric methane concentrations  
68 change almost in phase with abrupt Greenland climate change allowing for those events to be synchronized in  
69 ice cores. A weakness of the bipolar gas matching approach is the dependency on a precise determination of the  
70 so-called Δage that refers to the offset in age between the ice and the air enclosed in an ice core at a given depth  
71 (Blunier et al., 2007; Schwander and Stauffer, 1984). Modeling past Δage requires assumptions about past  
72 accumulation and temperature variations, introducing substantial age uncertainties associated with the  
73 synchronization.

74 Cosmogenic isotope production rates are modulated by the Earth's magnetic field and by solar variability, and  
75 they therefore carry a global signal that is shared by Greenland and Antarctic cosmogenic ice core records.  
76 Bipolar ice core synchronization using cosmogenic isotopes has mostly been done in the Holocene (Mekhaldi et  
77 al., 2015; Sigl et al., 2015; Steinhilber et al., 2012) and around the geomagnetic Laschamps event that occurred  
78 some 41 ka ago (Raisbeck et al., 2017; Raisbeck et al., 2007). Furthermore, the ice core cosmogenic signal enables



79 the comparison with  $^{14}\text{C}$  records of other archives, such as dendrochronologies (Adolphi and Muscheler, 2016;  
80 Sigl et al., 2016) and stalagmites (Adolphi et al., 2018). Weaknesses of this technique include the sparsity of  
81 significant events, climatic influences on radionuclide transport and deposition masking the cosmogenic signal,  
82 and the very costly and time-consuming analyses that limit the possibility of obtaining continuous high-resolution  
83 records. Furthermore, archive noise in the ice core records hampers unambiguous peak detection and  
84 synchronization.

85 This study focuses on volcanic bipolar synchronization of ice cores in the second half of the last glacial period  
86 (12-60 ka BP). The volcanic record of the last glacial period in Greenland ice cores includes more than a hundred  
87 confirmed Icelandic and high-latitude eruptions that have left predominantly cryptotephra (invisible to the naked  
88 eye) deposits in the ice (Abbott and Davies, 2012; Bourne et al., 2015) (Cook et al, in prep 2020); and presumably  
89 many more Icelandic eruptions that have not been identified as such. In addition to those, a large number of  
90 more distant eruptions have left an acidity signature in the ice cores but no tephra (Zielinski et al., 1997). In fact,  
91 during the last glacial only tephra from mid and high latitude eruptions have been identified in Greenland,  
92 whereas, to date, there is no evidence of tropical, low latitude or even continental European tephra in Greenland.  
93 Whether the lower latitude tephra never make it to Greenland or whether they are too small to be identified  
94 by conventional optical microscopy techniques and thus masked by more abundant, similar-sized background  
95 dust of continental origin is an open question.

96 In Antarctica, there are many visible tephra layers of Antarctic origin as well as a large number of acidity spikes  
97 associated with more distant eruptions (Narcisi et al., 2017; Severi et al., 2007). It has been proposed that tephra  
98 of tropical origin is present in the WAIS Divide ice core, but the evidence is solely based on dust size distributions  
99 and not on geochemical fingerprinting (Koffman et al., 2013). A pioneering study has suggested to have identified  
100 a bipolar tephra at around A.D. 1257 (Palais et al., 1992) and there is recent support for that conclusion  
101 suggesting that the source is the Indonesian Samalas volcano (Lavigne et al., 2013).

102 Although the ice-core records lack bipolar tephra layers they do hold evidence of volcanic eruptions that are  
103 powerful enough to leave sulfuric acid in the stratosphere from where it may be distributed to both Greenland  
104 and Antarctica. More than 80 such events have been identified for the last 2500 years (Sigl et al., 2015). For the  
105 earlier part of the Holocene, which has been less intensely studied, some 75 bipolar events have been found  
106 (Veres et al., 2013), and from around the time of the Indonesian Toba eruption occurring in Sumatra some 74 ka  
107 ago, a handful of bipolar volcanic events have been identified (Svensson et al., 2013). Recently, there has been  
108 progress in identifying stratospheric volcanic peaks in ice cores based on their sulfur isotopic fingerprints (Burke  
109 et al., 2019; Gautier et al., 2019). In this work, we expand the bipolar volcanic matching approach systematically  
110 throughout the 12-60 ka time interval.

## 111 2. Methods

112 The approach taken to synchronize Greenland and Antarctic ice cores is to identify large volcanic eruptions with  
113 a bipolar acidity or sulfur/sulfate signature. Because such events generally do not leave tephra in ice cores from  
114 both polar regions, individual eruptions cannot be matched geochemically between the two hemispheres, as  
115 there is no way to verify that they have the same source. What can be matched up, however, are sequences of  
116 eruptions that show the same relative timing in both Greenland and Antarctica. To determine the time interval  
117 between eruptions, and thereby the relative timing of events, annual layer counting is carried out over the  
118 volcanic sequence in both Greenland and Antarctic ice cores. When identical volcanic peak patterns are identified



119 in north and south, it is seen as a strong indication for a bipolar link. There is, however, always a risk of making  
120 an incorrect link, because an assumed volcanic sequence could consist of regional (non-bipolar) eruptions with  
121 coincidental similar temporal spacing.

122 The peak heights of the recorded eruption intensities in a bipolar volcanic ice-core sequence cannot be expected  
123 to be similar at the two poles, because the strength of the recorded signal depends on the geographical location  
124 of the eruption, the atmospheric circulation at the time of the eruption, and the variability in deposition of acids  
125 at the ice coring sites (Gautier et al., 2016). Furthermore, the annual layer counting comes with an uncertainty  
126 that adds to the possibility of making an incorrect bipolar match (Rasmussen et al., 2006). On the other hand,  
127 the bipolar timing of Greenland and Antarctic ice core records is already well constrained by existing gas- and  
128 <sup>10</sup>Be-based bipolar synchronizations. At the onset of each GI, the uncertainty in the bipolar methane matching  
129 between the Greenland NGRIP and the Antarctic WDC ice cores is around a century (Buizert et al., 2015), which  
130 constrains the time windows for matching of bipolar volcanic sequences. Similarly, the cosmogenic isotope link  
131 around the time of the Laschamps event firmly constrains the volcanic matching in that time period (Raisbeck et  
132 al., 2017). Therefore, the risk of making false bipolar volcanic matches is strongly reduced by the existing bipolar  
133 synchronization.

134 We perform annual layer counting in sections of the Greenland NGRIP (North Greenland Ice Core Project  
135 members, 2004) and the Antarctic EPICA (European Project for Ice Coring in Antarctica) Dronning Maud Land  
136 (EDML) (EPICA community members, 2006) ice cores using high-resolution records of chemical impurities (Bigler,  
137 2004; Ruth et al., 2008), dust (Ruth et al., 2003; Wegner et al., 2015), and visual grey-scale intensity (Faria et al.,  
138 2018; Svensson et al., 2005). The approach is the same as that applied for the glacial section of the Greenland  
139 Ice core Chronology 2005 (GICC05) (Andersen et al., 2006; Svensson et al., 2008). For this study, most sections  
140 of the NGRIP ice core have been recounted, and the Greenland time scale has been slightly modified as the  
141 bipolar matching allows for obtaining an improved precision from annual counting in both NGRIP and EDML. The  
142 EDML ice core has not previously been layer-counted in the glacial period, but for the investigated time interval  
143 the annual layer thicknesses are comparable to those of NGRIP (Veres et al., 2013) and layer counting can be  
144 done in a similar way. The two-core layer counting is not continuous, but is focused on periods of abrupt climate  
145 variability or high volcanic activity. In order to allow for comparison to published records ages in all tables and  
146 figures have been converted to GICC05 ages using the year 2000 CE as datum (referred to as 'b2k').

147 In order to obtain a robust identification of volcanic sequences in the ice cores, all available acidity records from  
148 the Greenland GRIP (Wolff et al., 1997), GISP2 (Mayewski et al., 1997), NGRIP (Bigler, 2004), and NEEM  
149 (Schüpbach et al., 2018) ice cores have been included. For Antarctica, records from the EDML ice core from the  
150 Atlantic sector (EPICA community members, 2006), the EDC core from the East Antarctic plateau (EPICA  
151 community members, 2004), and the West Antarctic Ice Sheet Divide (WDC) (Fudge et al., 2013; Sigl et al., 2016)  
152 ice core are used. Records of sulfur, sulfate, chloride, and Electrical Conductivity Measurements (ECM) of the ice  
153 (Hammer et al., 1980), Dielectric Profiling (DEP) (Moore et al., 1989; Wilhelms et al., 1998) and the liquid  
154 conductivity of melt water are also employed as good indicators of volcanic signals in ice cores. With the inclusion  
155 of those records, the ability of distinguishing large global volcanic events from more regional eruptions is  
156 improved, in particular for Antarctica.

157 The Greenland ice cores used here previously have been synchronized by volcanic events (Rasmussen et al.,  
158 2013; Seierstad et al., 2014). Likewise, the Antarctic ice cores have been linked internally by volcanic matching



159 (Buizert et al., 2018; Ruth et al., 2007). In addition to the published volcanic match points made for Antarctica,  
160 some 25 additional Antarctic match points have been identified in the present study to strengthen the  
161 synchronization in the neighborhood of Greenland abrupt climate change events. The non-bipolar or 'local'  
162 volcanic matching applied here is in agreement with the published synchronizations for Greenland and  
163 Antarctica, respectively.

164 To investigate the bipolar climate signal, we employ high-resolution stable water isotopes ( $\delta^{18}\text{O}$ ) from the GRIP  
165 (Johnsen et al., 2001), GISP2 (Stuiver and Grootes, 2000), NGRIP (Gkinis et al., 2014), and NEEM (Vinther et al.,  
166 in prep, 2020) ice cores, as well as  $\delta^{18}\text{O}$  and deuterium excess from the EDML (EPICA community members, 2006),  
167 EDC (EPICA community members, 2004) and WDC (Buizert et al., 2018) ice cores. The sources of the employed  
168 datasets are listed in Table S1.

### 169 3. Results

170 The bipolar volcanic match points identified in the 12-60 ka interval are shown in Fig. 1 and listed in Table 1. Of  
171 the 85 bipolar match points listed, five are previously published cosmogenic match points associated with the  
172 Laschamps geomagnetic excursion occurring in the 40.5-42.0 ka interval (Raisbeck et al., 2017). For the interval  
173 16.5-24.5 ka, roughly corresponding to the Last Glacial Maximum (LGM), the ice cores are notoriously difficult  
174 to match up, and no bipolar match points are reported. We note that most of the identified bipolar match points  
175 fall within Greenland interstadial periods and rather few are located in stadials. The main reasons for this are the  
176 elevated dust concentrations in the colder periods that mutes the ice conductivity signal as well as the elevated  
177 sulfuric background signal of colder periods that obscures the volcanic signal of the ice (Seierstad et al., 2014).  
178 Besides this, precise annual layer counting is also more difficult in the colder periods where accumulation is lower  
179 (Andersen et al., 2006).

180 All of the bipolar volcanic match points are identified in the Greenland NGRIP and the Antarctic EDML ice cores,  
181 and most of them are also identified in the Antarctic WDC and EDC ice cores. About half of the bipolar match  
182 points are also identified in the Greenland GRIP, GISP2, and NEEM ice cores, but the lower resolution of available  
183 sulfate and conductivity records for those cores is often insufficient for precise identification of weaker volcanic  
184 events. The Greenland ice cores are however internally synchronized throughout the last glacial period  
185 (Rasmussen et al., 2013; Seierstad et al., 2014) by northern hemispheric eruptions, typically Icelandic in origin,  
186 that leave a stronger fingerprint in Greenland. Therefore, for most of the bipolar match points all of the  
187 Greenland ice cores are precisely matched by interpolation between Greenland match points.

188 The bipolar match points are unevenly distributed over the 12-60 ka interval, but bipolar volcanic events have  
189 been identified within a range of 500 years of all major onsets and terminations of Greenland interstadials (GIs)  
190 with the exception of GI-2 (Fig. 1). All of the Greenland abrupt climate-change events in that period (except for  
191 GI-2) are thus synchronized with the Antarctic climate at high precision. The derived depths and ages for the  
192 onsets and terminations of GI events are shown in Table 2. Based on the 5% average counting uncertainty during  
193 the last glacial period (Svensson et al., 2008), the relative uncertainty of the bipolar linking related to the GI  
194 events is taken as 10% of the distance to the nearest bipolar match point (Table 2). On average, this relative  
195 uncertainty is less than 15 years and reaches a maximum of 50 years. The definition of GI onsets and terminations  
196 applied in this study are the midpoints of the NGRIP isotopic transitions as identified in Buizert et al. (2015),  
197 except for the onset of GI-1 (the Bølling-Allerød) which is taken from Steffensen et al. (2008).



198 In the following sections, we provide examples of the bipolar synchronization from selected time intervals. In the  
199 supplementary material detailed figures are provided for all the DO events (Fig. S1-S14).

### 200 **3.1 The termination of GI-1 / Onset of the Younger Dryas**

201 The onset of the Younger Dryas (GS-1) is synchronized between the two hemispheres by four large acidity spikes  
202 clustered around 13 ka and spanning 110 years (Fig. 2). The two outermost spikes are most significant, but all  
203 four spikes are present in all investigated cores. All four volcanic eruptions are interpreted as bipolar and they  
204 are therefore most likely associated with low-latitude eruptions. This is in conflict with the hypothesis that one  
205 of them should be related to the German Laacher See eruption (Baldini et al., 2018) that is believed to have a  
206 primarily Northern Hemispheric fingerprint (Graf and Timmreck, 2001). A tephra layer in the NGRIP ice core  
207 occurring close to the oldest of the four spikes has previously been tentatively associated with a Hekla eruption  
208 (Mortensen et al., 2005), but with the clear bipolar signature there is likely a temporal overlap between this  
209 Icelandic and an additional lower-latitude eruption. We notice that the eruption associated with the very  
210 significant North Atlantic Vedde Ash layer (Lane et al., 2012; Mortensen et al., 2005) located at 12.17 ka in the  
211 Greenland ice cores (Rasmussen et al., 2006) potentially has left a weak acidic signal in Antarctica.

212 Our bipolar volcanic linking allows for synchronizing the climate signal of the investigated cores (Figure 3). The  
213 four Greenland cores show quite variable climate patterns for the termination of GI-1, making it difficult to define  
214 the duration of the transition, but they all have the most significant drop in isotopic values in the interval  
215 constrained by the two bipolar events at 12.75 ka and 12.92 ka, respectively. The Antarctic cores show a fairly  
216 constant isotope level in the 12.75 – 13.25 ka interval followed by a rise in isotopic values starting around 12.75  
217 ka.

218 It has been proposed that the Younger Dryas period/GS-1 was initiated by a cosmic impact for which there is  
219 indirect and debated evidence in a large number of sites in the NH surrounding the North Atlantic region (Kennett  
220 et al., 2015). A very significant Platinum (Pt) spike has been identified in the GISP2 ice core (Petaev et al., 2013)  
221 and at several North American sites (Moore et al., 2017) that potentially originate from the same impact event.  
222 The Pt spike occurs about 45 years after the volcanic quadruplet, i.e. after the Greenland cooling has initiated  
223 but before it has reached its minimum (Fig. S1B). The hypothesis of the YD initiation by a cosmic impact is debated  
224 (Holliday et al., 2020), and it recently took an exciting twist with the discovery of the (undated) Hiawatha impact  
225 crater in NW Greenland (Kjær et al., 2018). Based on ice radar profiles and other evidence, the crater, which is  
226 located 378 km from the NEEM drill site, has been suggested to be the origin of the YD impact event. From an  
227 ice core point of view, however, we would expect the ice core stratigraphy to be significantly affected by such a  
228 dramatic event occurring in Greenland. Yet, we do not find any signs of disturbances of the ice core stratigraphy  
229 at the time of the GISP2 Pt spike. The annual layers are well preserved in all Greenland cores, and there is no  
230 abnormal layer thickness nor any elevated concentrations of dust or other impurities. Our study thus gives no  
231 support for the Hiawatha crater to have formed close to the onset of YD/GS-1; nor for the onset of the YD to  
232 have been triggered by this impact.

### 233 **3.2 The onset of Greenland Interstadial 1 (GI-1) / Bølling-Allerød**

234 The very steep Greenland onset of the GI-1 / Bølling-Allerød period is preceded by a 1.8 ky-long period of strong  
235 global volcanic activity (Fig. S2A). The bipolar phasing is well constrained by several significant eruptions leading  
236 up to the onset, and the bipolar volcanic matching pattern is easily recognized. In agreement with Steffensen et



237 al. (2008), we note that NGRIP appears to be the Greenland ice core with the steepest  $\delta^{18}\text{O}$  transition at the GI-  
238 1 onset (Fig. S2B). The Antarctic ice cores are all peaking close to 200 years after the Greenland mid-transition in  
239 agreement with the methane matching of NGRIP and WDC (Buizert et al., 2015). The very strong volcanic double  
240 spike in NGRIP close to 15.68 ka is associated with tephra from the explosive caldera-forming Towada-H eruption  
241 (Bourne et al., 2016) located in present-day Japan close to 40°N. This eruption appears to have no significant  
242 Antarctic imprint.

### 243 3.3 Greenland Stadial 3 (GS-3)

244 In the late GS-3, at 24.67 ka, there is a characteristic volcanic triplet spike that constitutes a strong bipolar link  
245 (Fig. S3A). The three spikes are separated by  $20\pm 1$  and  $10\pm 1$  years, respectively, making the match point unique.  
246 At 25.46 ka (b2k GICC05 age) we hypothesize to record in Greenland traces from the Oruanui eruption from the  
247 Taupo volcano in present-day New Zealand in the Greenland record. Tephra of this eruption has been previously  
248 identified and dated to 25.37 ka (b2k WD2014 age) in the WDC ice core (Dunbar et al., 2017). There appears to  
249 be a major Greenland acidity spike associated with this eruption despite its latitude being close to 40°S.  
250 Unfortunately, there are no adjacent bipolar eruptions within several hundreds of years making the bipolar  
251 Oruanui link somewhat uncertain. The nearest pair of bipolar eruptions is found at 25.76 and 25.94 ka,  
252 respectively, leaving enough room in the layer counting uncertainty for the Greenland acidity spike to potentially  
253 be a 'false match' offset by up to 30 years from the Antarctic Oruanui spike. The link needs to be investigated by  
254 the bipolar sulfur isotopes method to rule out a coeval local source for the NGRIP event (Burke et al., 2019).  
255 Besides the potential bipolar link, the Oruanui eruption is also relevant for comparing Greenland and Antarctic  
256 ice core time scales (Sigl et al., 2016) and it constitutes an important comparison point for  $^{14}\text{C}$  ages and ice core  
257 chronologies (Muscheler et al., In review, February 2020).

### 258 3.4 The onset of Greenland Interstadial 8 (GI-8)

259 The very prominent onset of GI-8 is associated with four significant bipolar eruptions within a 400 yr period (Fig.  
260 2). The eruption occurring at 38.13 ka, close to a century after the onset, shows a very significant signal in all  
261 acidity proxies of all investigated ice cores, and it appears to be one of the largest eruptions of the last glacial  
262 period. We thus see it as a potential candidate for the H1 horizon identified in Antarctica by radio-echo sounding  
263 (Winter et al., 2019). Other prominent bipolar events are situated at 37.97, 38.23, and 38.37 ka, respectively.  
264 The 38.23 ka event occurs right at the initiation of the GI-8 onset.

265 In the climate records across the GI-8 onset, the Greenland records behave quite similarly, whereas the Antarctic  
266 records show rather distinct patterns (Fig. 3). EDC expresses a prominent warming coinciding with the Greenland  
267 warming; WDC also shows a warming although much less significant. Both EDC and WDC exhibit a cooling trend  
268 initiating some decades after the Greenland onset. In contrast, EDML shows a century-long cooling period  
269 starting right at the Greenland onset. Being rather noisy, it is hard to separate signal from noise in the Antarctic  
270 records based on just one warming event. However, the stacking exercise across several warming events  
271 discussed below reveals that the pattern expressed by the Antarctic records at the GI-8 onset is an archetypical  
272 expression of an Antarctic response to a major GI onset.

### 273 3.5 Greenland interstadials 9 and 10 (GI-9 and GI-10)

274 For the period 40-43 ka that covers GI-9 and GI-10, the bipolar matching is very well constrained by 16 bipolar  
275 match points (Fig. S8A), five of which are independent cosmogenic match points related to the Laschamps



276 geomagnetic excursion (Raisbeck et al., 2017). The volcanic match presented here is in agreement within  
277 uncertainties with the cosmogenic matching, and it replaces the existing bipolar volcanic matching in this region  
278 (Svensson et al., 2013) that has been shifted by some 30 years.

279 The onsets of GI-9 and GI-10 provide examples of less prominent GI-events where the Antarctic isotopic response  
280 pattern is different from that of the larger events, such as GI-8 and GI-12 (Fig. S8B). For the GI-9 onset, it is  
281 practically impossible to distinguish a bipolar seesaw response in the adjacent periods in the Antarctic climate  
282 records. For the GI-10 onset, EDC has a small spike and EDML has a dip, but none of them stand out from the  
283 background. WDC appears to enter GI-10 without any climatic response. For the smaller/weaker GI events the  
284 response pattern in Antarctica is likewise smaller, making it harder to identify it within the isotopic background  
285 variability (Fig. 1).

#### 286 **4. Bipolar phasing of abrupt climate change**

287 The characteristics of the climate record of the individual GI onsets may vary from event to event, from ice core  
288 to ice core and from proxy to proxy both in Greenland and in Antarctica. In Greenland, the main pattern  
289 associated with a GI onset is similar for all deep ice cores, but transition durations and the relative phasing of  
290 individual parameters, such as water isotopes and impurity concentrations, vary between events and to a lesser  
291 degree between cores (Erhardt et al., 2019; Rasmussen et al., 2014; Steffensen et al., 2008). In Antarctica, the  
292 investigated cores are located further apart, they are exposed to the climatic influence from different ocean  
293 basins, and they do in general show greater variability in relation to the Greenland GI onsets than is the case for  
294 the more closely located Greenland coring sites. Millennial-scale climate variability in Antarctica furthermore has  
295 a profoundly lower signal-to-noise ratio than that in Greenland, contributing to the difficulty of interpreting  
296 individual events.

297 Keeping in mind this variability among individual GI events, we find it useful to extract a general pattern across  
298 the GI onsets and terminations by aligning the individual events and stacking (or compositing) them, as it has  
299 been done using bipolar methane synchronization (Buizert et al., 2015; Buizert et al., 2018). The stacking provides  
300 us with an overall phasing relation that may be helpful in unravelling the governing mechanisms of the abrupt  
301 climate change, for example by comparison to model experiments that typically do not capture the details of  
302 individual events (Buizert et al., 2018). We stress that the associated underlying assumption of the stacking  
303 approach, that the complete temporal progression of all events is the result of the same underlying process, may  
304 not be fully justified.

305 In Fig. 4, we show the  $\delta^{18}\text{O}$  records of NGRIP together with five Antarctic ice cores stacked across all of the GI  
306 onsets and terminations in the 12-60 ka interval (except for GI-2), centered at the Greenland transition midpoint  
307 as defined in Table 2. Besides the EDML, EDC and WDC ice cores applied for the bipolar synchronization in this  
308 study, we expand the geographical coverage by including the Antarctic Dome Fuji (DF)(Kawamura et al., 2007)  
309 and Talos Dome (TAL)(Stenni et al., 2010) records applying the existing Antarctic volcanic synchronization  
310 (Buizert et al., 2018; Fujita et al., 2015; Severi et al., 2012). Fig. 5 shows the stacking of the five Antarctic ice cores  
311 from Fig. 4, thus a stack of 21 events in five Antarctic ice cores totaling 105 events. We note that the Greenland  
312 onsets are aligned according to the midpoint of the warming transition (set to  $t=0$ ), implying that the initiation  
313 of the Greenland event occurs earlier than the alignment point. A recent study suggests that the abrupt NGRIP  
314  $\delta^{18}\text{O}$  and Calcium (Ca) transition onsets on average precede the  $\delta^{18}\text{O}$  transition midpoint by  $25\pm 7$  and  $33\pm 15$



315 years, respectively (Erhardt et al., 2019); in Fig. 4 and Fig. 5 this places the Greenland  $\delta^{18}\text{O}$  and Ca event onsets  
316 at  $t = -25$  and  $t = -33$  years, respectively.

317 For Antarctica, the stacked EDC, WDC and EDML records show distinct  $\delta^{18}\text{O}$  patterns similar to those identified  
318 for the onset of GI-8 (Fig. 3). EDC, WDC and TAL show a peak of accelerated warming, the onset of which is  
319 synchronous with Greenland warming and that lasts for close to a century. DF likewise shows an accelerated  
320 warming, albeit somewhat later than the aforementioned cores. This direct Antarctic warming response to the  
321 Greenland warming is likely to be associated with fast atmospheric changes on a global scale (Markle et al., 2017).  
322 In particular, it has been proposed that a northward shift in the SH westerlies in response to NH warming (Lee et  
323 al., 2011; Pedro et al., 2018) may drive a warming anomaly in most of the Antarctic continent through enhanced  
324 zonal heat transport in the atmosphere (Buizert et al., 2018; Marshall and Thompson, 2016). Another process  
325 that is likely to contribute to the alignment of the water isotope records at the GI onsets is the local cycle of  
326 sublimation-condensation in summer on the Greenland and Antarctic ice sheets that is currently under  
327 investigation (Kocec et al., 2019; Pang et al., 2019).

328 EDML, however, shows an immediate cooling response that is distinct among the cores investigated (Fig. 4 and  
329 Fig. S15), perhaps reflecting regional effects such as wind-driven changes to the Weddell Sea stratification, gyre  
330 circulation, sea-ice extent or polynya activity.

331 Based on the volcanic bipolar synchronization, the general Antarctic response time (Fig. 5) to a Greenland  
332 warming event is shorter than that obtained from bipolar methane linking (Buizert et al., 2015). Instead of the  
333 200 year lag found in the methane-based synchronization, we find an average response time of  $122 \pm 24$  years  
334 ( $2\sigma$  uncertainty) using the same fitting routine as used in Buizert et al. (2015) (see discussion of uncertainty  
335 estimates below). This difference is mostly due to uncertainty in the WDC  $\Delta$ age calculation; the new  
336 synchronization suggests that the glacial  $\Delta$ age was too small by around 70 years on average (Fig. S16).

337 Besides  $\delta^{18}\text{O}$ , we also stack records of Antarctic deuterium excess using the logarithmic definition ( $d_{\text{in}}$ ) introduced  
338 by (Uemura et al., 2012). Previous work has found  $d_{\text{in}}$  to abruptly increase (decrease) in synchrony with the onset  
339 (termination) of GIs at multiple Antarctic sites (Buizert et al., 2018; Markle et al., 2017; Masson-Delmotte et al.,  
340 2010), which has been attributed to shifts of the Southern Hemisphere (SH) subpolar jet and westerly winds (e.g.  
341 Schmidt et al. (2007)). Stacks using a methane-based synchronization show a  $d_{\text{in}}$  transition that takes  $\sim 220$  years,  
342 followed by a broad peak (Fig. 5); in contrast, our volcanic synchronization suggests a shorter transition ( $152 \pm$   
343  $37$  years) and a much sharper  $d_{\text{in}}$  transition. Any chronological errors in the bipolar synchronization will misalign  
344 the events being composited, thereby broadening the climatic features in the stacked record. The fact that our  
345 volcanic synchronization yields sharper features is thus indirect evidence that it is more accurate than existing  
346 gas-based synchronizations. The duration of the  $d_{\text{in}}$  transition we observe in our stack is still an upper bound on  
347 its true duration, given that our event alignment includes uncertainties due to annual layer counting to the  
348 nearest volcanic tie point, as well as potentially incorrectly identified volcanic tie points. It was suggested that  
349 the gradual  $d_{\text{in}}$  trends before and after the transition follow the gradual source-water sea-surface-temperature  
350 trends of the SH via the bipolar seesaw (Markle et al., 2017).

351 Our volcanic bipolar synchronization also shifts the onset of the  $d_{\text{in}}$  transition towards older ages, placing it at  $t$   
352  $= -30 \pm 29$  years ( $2\sigma$  uncertainty) relative to the Greenland  $\delta^{18}\text{O}$  transition midpoint. Such an early onset may  
353 seem surprising, but is actually in very good agreement with other Greenland proxies that suggest that low-



354 latitude changes precede the Greenland  $\delta^{18}\text{O}$  signals. In particular, changes in Greenland dust / Ca concentrations  
355 appear to lead the Greenland  $\delta^{18}\text{O}$  by a decade at the onset of the transitions (Erhardt et al., 2019), which has  
356 been attributed to early changes in the ITCZ position and atmospheric circulation (Steffensen et al., 2008).  
357 Meridional shifts in the SH eddy-driven jet and westerlies are suggested to be dynamically linked to the ITCZ  
358 position (Ceppi et al., 2013). The onset of the Greenland Ca transition (presumably reflecting NH atmospheric  
359 circulation shifts) precedes the Greenland  $\delta^{18}\text{O}$  transition midpoint (which we set as  $t=0$ ) by  $33 \pm 15$  years on  
360 average (Erhardt et al., 2019), in good agreement with the  $30 \pm 29$  years we find for the onset of SH atmospheric  
361 circulation changes.

362 The Antarctic  $d_{in}$  and  $\delta^{18}\text{O}$  signals (Fig. 5) are recorded in the same physical ice core, and therefore the uncertainty  
363 in their relative phasing is small. Errors in the bipolar synchronization will blur the abruptness of their transitions,  
364 but should not alter their relative phasing; by contrast, the phasing relative to Greenland proxies is very sensitive  
365 to bipolar synchronization errors. The  $152 \pm 37$  year duration between the onset of the  $d_{in}$  response, and the  
366 breakpoint in the  $\delta^{18}\text{O}$  curve therefore represents a robust estimate of the climatic lag of the mean Antarctic  
367 temperature response behind the first atmospheric manifestation of the GI event in the southern hemisphere  
368 high latitudes.

369 At the terminations of GI events, the stacked NGRIP  $\delta^{18}\text{O}$  shows a less prominent but still sharp transition over a  
370  $\sim 100$  year interval (Fig. 4). For  $\delta^{18}\text{O}$ , all of the stacked Antarctic cores reach a minimum in the interval 100-150  
371 year following the Greenland termination with the strongest response seen for TAL. For  $d_{in}$ , EDC and DF show a  
372 significant response related to the Greenland terminations, whereas the other Antarctic cores express a less  
373 coherent signal. Note that EDML has its coldest temperatures near  $t=0$ , suggesting again a fast response at this  
374 site of opposite sign as in the DO warming case.

#### 375 4.1 Uncertainty estimate of stacked records

376 To estimate the uncertainty in the change-point analysis of the stacked records (Fig. 5) we use a Monte Carlo  
377 scheme with 1,000 iterations (Buizert et al., 2015). In each iteration, the alignment of the individual events is  
378 shifted randomly prior to the stacking, and the change-point is identified in the new stack using an automated  
379 algorithm. The applied time shifts are randomly drawn from normal distribution with widths corresponding to  
380 the following event-specific uncertainties; (1) the uncertainty in the NGRIP event midpoint detection (Buizert et  
381 al., 2015); (2) the uncertainty in the Antarctic layer count from the bipolar eruption to the event (Table 2a); (3)  
382 the uncertainty in the Antarctic volcanic synchronization (Buizert et al., 2018). In each iteration, the user-  
383 specified parameters of the fitting algorithm (such as the time interval used in the fitting) are likewise perturbed  
384 randomly. The stated  $2\sigma$  uncertainty values therefore reflect uncertainty in the bipolar synchronization, stacking  
385 procedure, and change-point detection.

386 The Antarctic delay times and uncertainties identified for  $\delta^{18}\text{O}$  and  $d_{in}$ , respectively, are valid for the stacked  
387 (averaged) transitions (Fig. 5), but are not representative for the variation among individual transitions. When  
388 performing an event-by-event fitting of the Antarctic 5-core average we find a much greater range of delay times.  
389 For the  $\delta^{18}\text{O}$  change point, the mean and standard deviation of the individual-event timings is  $t = 138 \pm 89$  years;  
390 for the  $d_{in}$  it is  $-6 \pm 78$  years and  $116 \pm 80$  years for transition beginning and end, respectively. This larger variability  
391 reflects both differences in timing between individual events, as well as the much smaller signal-to-noise ratio  
392 when fitting individual events.



## 393 5. Conclusions and outlook

394 Overall, our new bipolar volcanic synchronization confirms the centennial-scale delay of the mean Antarctic  
395 bipolar seesaw temperature response behind abrupt Greenland DO variability (Buizert et al., 2015); however,  
396 the improved age control offered by volcanic synchronization significantly reduces the estimated duration of this  
397 delay compared to previous work based on CH<sub>4</sub> synchronization. Our reduced estimates are more in line with,  
398 but still larger than, results from climate model simulations (Pedro et al., 2018; Vettoretti and Peltier, 2015), that  
399 typically give an oceanic response on multi-decadal timescales.

400 WAIS Divide Project Members (2015) interpreted the  $208 \pm 96$  year delay they observed as characteristic of an  
401 oceanic teleconnection. The reduced delay timescale we infer here ( $122 \pm 24$  years) is still consistent with the  
402 original interpretation. However, the new observations urge some caution. Despite our best efforts, the new  
403 bipolar volcanic framework likely contains some incorrect matches, and as the bipolar synchronization continues  
404 to be refined, the inferred Antarctic delay may be reduced further. The divergent climate response at various  
405 sites (Fig. 4, Fig. S15 and Buizert et al. (2015)), as well as the relatively gradual transition in  $d_{in}$  over  $\sim 145$  years  
406 (suspiciously similar to the updated timescale Antarctic temperature delay presented here) perhaps suggest a  
407 more complex interplay of atmospheric and oceanic processes that is currently very poorly understood (see e.g.  
408 Kostov et al. (2017)). We suggest future work along two parallel lines of inquiry.

409 First, further refinement and confirmation of our bipolar synchronization is called for. Analysis of sulfur mass-  
410 independent isotopic fractionation (Burke et al., 2019) is needed for the proposed bipolar volcanic events. For  
411 low-latitude eruptions to show up in both the Arctic and Antarctic almost certainly requires injection of materials  
412 into the stratosphere, which is reflected in  $\Delta^{33}\text{S}$ . High-resolution records of  $^{10}\text{Be}$  can further refine bipolar  
413 matching (Adolphi et al., 2018) in critical intervals where the volcanic record is ambiguous. Second, climate  
414 modeling studies are needed to better understand the interaction between atmospheric and oceanic changes  
415 during the D-O cycle. In particular the anomalous response of the EDML site during both Heinrich (Landais et al.,  
416 2015) and Dansgaard-Oeschger (Buizert et al., 2018) abrupt climate change calls for detailed investigation.

417 The volcanic bipolar synchronization has a wide range of potential applications that go beyond the objectives of  
418 this paper. Those include the development of consistent bipolar ice core time scales, constraining ice-core delta-  
419 gas ages, investigation of impacts of volcanism on abrupt climate change, quantification of the last glacial global  
420 volcanic eruption record, and the discussion of solar variability through synchronization of cosmogenic isotopes.  
421 Furthermore, the precise bipolar synchronization should allow for an improved understanding of the  
422 mechanisms governing the glacial climate through comparison to model studies and non-ice core records.

### 423 Author contribution

424 All authors contributed to obtaining the applied datasets. AS prepared the manuscript with contributions from  
425 all co-authors. CB prepared Figures 4 and 5.

### 426 Competing interests

427 The authors declare that they have no conflict of interest.

### 428 Acknowledgments



429 This project has received funding from the European Union’s Horizon 2020 research and innovation programme  
430 under grant agreement No 820970 (TiPES) and from the Villum Investigator Project IceFlow (No. 16572). Buizert  
431 gratefully acknowledges financial support from the US National Science Foundation (ANT- 1643394). Rasmussen  
432 and Capron gratefully acknowledges support from the Carlsberg Foundation to the ChronoClimate project.  
433 Adolphi was supported by the Swedish Research Council (Vetenskapsrådet DNr. 2016-00218). Muscheler was  
434 partially supported by the Swedish Research Council (grant DNR2013-8421). Sigl acknowledges funding from the  
435 European Research Council (ERC) under the European Union’s Horizon 2020 research and innovation programme  
436 (grant agreement 820047). Stocker and Fischer acknowledge the long-term support of ice core research at the  
437 University of Bern by the Swiss National Science Foundation (grants 200020\_172745, 200020\_172506). US NSF  
438 grants 0839093 and 1142166 to McConnell supported measurements in the WAIS Divide core. The NEEM ice  
439 coring project was directed and organized by the Center of Ice and Climate at the Niels Bohr Institute and US  
440 NSF, Office of Polar Programs. It is supported by funding agencies and institutions in Belgium (FNRS-CFB and  
441 FWO), Canada (NRCan/GSC), China (CAS), Denmark (FIST), France (IPEV, CNRS/INSU, CEA and ANR), Germany  
442 (AWI), Iceland (Rannls), Japan (NIPR), Korea (KOPRI), The Netherlands (NWO/ALW), Sweden (VR), Switzerland  
443 (SNF), United Kingdom (NERC) and the USA (US NSF, Office of Polar Programs).

#### 444 **TABLE CAPTIONS:**

##### 445 **Table 1: Bipolar match points**

446 Depths and ages of bipolar volcanic and cosmogenic match points. GICC05 and WD2014 (Sigl et al., 2016) ages  
447 are provided with reference to year 2000 CE. Fields are empty when no match point has been identified. Five  
448 match points around GI-10 (BeA – BeE) are based cosmogenic bipolar matching (Raisbeck et al., 2017), all other  
449 match points are volcanic match points of this study. All EDC depths are on the EDC99 depth scale.

##### 450 **Table 2a + 2b: Bipolar onsets and terminations**

451 Depths of the Greenland interstadial onsets (a) and terminations (b) in the NGRIP, NEEM, GRIP, GISP2, EDML,  
452 EDC, and WDC ice cores based on volcanic matching. The NGRIP onsets are defined as the mid-points of the  $\delta^{18}\text{O}$   
453 transitions and are identical to those applied in Buizert et al. (2015) except for the onset of GI-1. The Greenland  
454 match points are from Seierstad et al. (2014), Antarctic match points are from Buizert et al. (2018), and the  
455 bipolar match points are from Table 1. Corresponding GICC05 ages are provided with reference to year 2000 CE.  
456 ‘Distance’ refers to the temporal distance to the nearest bipolar match point in Table 1 with negative values  
457 signifying the match point occurring before the onset/termination. The relative uncertainty of the bipolar  
458 matching is stated as 10% of the ‘distance’ assuming a 5% maximum counting error of the annual layer counting  
459 in both Greenland and Antarctica. ‘YD-PB’ refers to the Younger Dryas – Preboreal transition (the onset of the  
460 Holocene) and ‘BA-YD’ refers to the Bølling-Allerød – Younger Dryas transition (the onset of GS-1). All EDC depths  
461 are on the EDC99 depth scale.

#### 462 **FIGURE CAPTIONS:**

##### 463 **Figure 1:**

464 Greenland (NGRIP) and Antarctic (EDML, WDC, and EDC) climate records ( $\delta^{18}\text{O}$ ) throughout the 10-60 ka time  
465 period based on volcanic matching. Ages are on the GICC05 time scale relative to the year 2000 CE (‘b2k’). Grey  
466 vertical lines show the position of bipolar volcanic match points identified in this study (Table 1) together with



467 five match points based on cosmogenic isotopes around 41 ka (Raisbeck et al., 2017). Blue-shaded intervals  
468 indicate the Greenland Interstadial (GI) periods according to the definition of Rasmussen et al. (2014). The bipolar  
469 synchronization for the 16.5-24.5 ka interval is tentative as there are no bipolar match points in that interval.

470 **Figure 2:**

471 Bipolar volcanic synchronization of the investigated ice cores across the transition from GI-1 / Bølling-Allerød  
472 (BA) to GS-1 / Younger Dryas (YD) (left panel) and the onset of GI-8 (right panel). Grey vertical lines are bipolar  
473 volcanic match points (Table 1). The records have different units, some are uncalibrated and peak heights are  
474 not comparable on an absolute scale, which is the reason why no scales are provided.

475 **Figure 3:**

476 Synchronized climate records of the investigated ice cores across the GS-1 onset (left panel) and the GI-8 onset  
477 (right panel) applying the volcanic synchronization shown in Fig. 2. The acidity records in the bottom of the figure  
478 are for reference and are also shown in Fig. 2. All other records are  $\delta^{18}\text{O}$  in ‰ (see Fig. 1 for scales). Grey vertical  
479 lines are bipolar volcanic match points (Table 1).

480 **Figure 4:**

481 Stacks of isotopic records across GI onsets (left) and terminations (right) for the events listed in Table 2a and 2b,  
482 respectively, applying the bipolar volcanic synchronization. The time 't=0' refers to the midpoint of the NGRIP  
483 onset for each GI-event as defined in Table 2. **Top:** Stack of NGRIP  $\delta^{18}\text{O}$  (blue; left axis) and WDC  $\text{CH}_4$  (green; right  
484 axis). **Center:** Stack of Antarctic  $\delta^{18}\text{O}$  at the indicated locations and the average curve (mean). **Bottom:** Stack of  
485 Antarctic  $d_{\text{in}}$  at the indicated locations and the mean. The figure is modified from Buizert et al. (2018), Extended  
486 data Fig. 3. See Fig. S15 for Antarctic core site locations.

487 **Figure 5:**

488 **Top:** Stack of Greenland NGRIP isotopes and  $\text{CH}_4$  for the onsets of GI events listed in Table 2a. **Center:** Antarctic  
489 5-core mean  $\delta^{18}\text{O}$  (stack of 5 x 21 warming events). Black curve is the same as 'mean' in Fig. 4 center; grey curve  
490 is applying the bipolar methane synchronization of Buizert et al. (2015). **Bottom:** Antarctic 5-core mean  
491 deuterium excess ( $d_{\text{in}}$ ). Black curve is the same as 'mean' in Fig. 4 bottom; grey curve is applying the bipolar  
492 methane synchronization of Buizert et al. (2015). Orange curves are fitting functions using the change-point  
493 analysis applied in Buizert et al. (2015). The stated  $2\sigma$  uncertainty estimates are obtained from a Monte Carlo  
494 sampling (see main text). When the same uncertainty estimate is made for the GI terminations (Fig. 4) the  $\delta^{18}\text{O}$   
495 timing is at  $101 \pm 29$  years, the  $d_{\text{in}}$  transition onset is at  $-59 \pm 58$  years, the  $d_{\text{in}}$  transition end is at  $95 \pm 34$  years;  
496 the duration between the  $d_{\text{in}}$  onset and the  $\delta^{18}\text{O}$  change-point is  $160 \pm 65$  years. The earlier  $d_{\text{in}}$  onset for the GI  
497 termination is probably reflecting that the GI terminations are generally more gradual than the GI onsets.

498



499 **REFERENCES:**

- 500 Abbott, P. M. and Davies, S. M.: Volcanism and the Greenland ice-cores: the tephra record, *Earth-Sci. Rev.*, 115,  
501 173-191, 2012.
- 502 Adolphi, F. and Muscheler, R.: Synchronizing the Greenland ice core and radiocarbon timescales over the  
503 Holocene - Bayesian wiggle- matching of cosmogenic radionuclide records, *Clim. Past.*, 12, 15-30, 2016.
- 504 Adolphi, F., et al.: Connecting the Greenland ice-core and U/Th timescales via cosmogenic radionuclides:  
505 testing the synchronicity of Dansgaard-Oeschger events, *Clim. Past.*, 14, 1755-1781, 2018.
- 506 Andersen, K. K., et al.: The Greenland Ice Core Chronology 2005, 15-42 ka. Part 1: constructing the time scale,  
507 *Quaternary Science Reviews*, 25, 3246-3257, 2006.
- 508 Baldini, J. U. L., Brown, R. J., and Mawdsley, N.: Evaluating the link between the sulfur-rich Laacher See volcanic  
509 eruption and the Younger Dryas climate anomaly, *Clim. Past.*, 14, 969-990, 2018.
- 510 Bender, M., Sowers, T., Dickson, M.-L., Orchardo, J., Grootes, P., Mayewski, P. A., and Meese, D. A.: Climate  
511 correlations between Greenland and Antarctica during the last 100,000 years, *Nature*, 372, 663-666,  
512 1994.
- 513 Bigler, M.: Hochauflösende Spurenstoffmessungen an polaren Eisbohrkernen: Glazio-chemische und  
514 klimatische Prozessstudien, 2004.Ph.D. dissertation, Physics Institute, University of Bern, Switzerland,  
515 2004.
- 516 Blunier, T., et al.: Asynchrony of Antarctic and Greenland climate change during the last glacial period, *Nature*,  
517 394, 739-743, 1998.
- 518 Blunier, T., Spahni, R., Barnola, J.-M., Chappellaz, J., Loulergue, L., and Schwander, J.: Synchronization of ice  
519 core records via atmospheric gases, *Clim. Past.*, 3, 325-330, 2007.
- 520 Bourne, A. J., Abbott, P. M., Albert, P. G., Cook, E., Pearce, N. J. G., Ponomareva, V., Svensson, A., and Davies, S.  
521 M.: Underestimated risks of recurrent long-range ash dispersal from northern Pacific Arc volcanoes,  
522 *Scientific Reports*, 6, 2016.
- 523 Bourne, A. J., Cook, E., Abbott, P. M., Seierstad, I. K., Steffensen, J. P., Svensson, A., Fischer, H., Schupbach, S.,  
524 and Davies, S. M.: A tephra lattice for Greenland and a reconstruction of volcanic events spanning 25-45  
525 ka b2k, *Quaternary Science Reviews*, 118, 122-141, 2015.
- 526 Buizert, C., et al.: Precise inter-polar phasing of abrupt climate change during the last ice age, *Nature*, 520, 661-  
527 U169, 2015.
- 528 Buizert, C., et al.: Abrupt ice-age shifts in southern westerly winds and Antarctic climate forced from the north,  
529 *Nature*, 563, 681-685, 2018.
- 530 Burke, A., Moore, K. A., Sigl, M., Nita, D. C., McConnell, J. R., and Adkins, J. F.: Stratospheric eruptions from  
531 tropical and extra-tropical volcanoes constrained using high-resolution sulfur isotopes in ice cores, *Earth  
532 Planet. Sci. Lett.*, 521, 113-119, 2019.
- 533 Capron, E., et al.: Synchronising EDML and NorthGRIP ice cores using delta O-18 of atmospheric oxygen (delta  
534 O-18(atm)) and CH4 measurements over MIS5 (80-123 kyr), *Quaternary Science Reviews*, 29, 222-234,  
535 2010.
- 536 Ceppi, P., Hwang, Y. T., Liu, X., Frierson, D. M. W., and Hartmann, D. L.: The relationship between the ITCZ and  
537 the Southern Hemispheric eddy-driven jet, *Journal of Geophysical Research Atmospheres*, 118, 5136-  
538 5146, 2013.
- 539 Dansgaard, W., et al.: Evidence for general instability of past climate from a 250-kyr ice-core record, *Nature*,  
540 364, 218-220, 1993.
- 541 Dunbar, N. W., Iverson, N. A., Van Eaton, A. R., Sigl, M., Alloway, B. V., Kurbatov, A. V., Mastin, L. G., McConnell,  
542 J. R., and Wilson, C. J. N.: New Zealand supereruption provides time marker for the Last Glacial Maximum  
543 in Antarctica, *Scientific Reports*, 7, 2017.



- 544 EPICA community members: Eight glacial cycles from an Antarctic ice core, *Nature*, 429, 623-628, 2004.  
545 EPICA community members: One-to-one coupling of glacial climate variability in Greenland and Antarctica,  
546 *Nature*, 444, 195-198, 2006.  
547 Erhardt, T., Capron, E., Rasmussen, S. O., Schupbach, S., Bigler, M., Adolphi, F., and Fischer, H.: Decadal-scale  
548 progression of the onset of Dansgaard-Oeschger warming events, *Clim. Past.*, 15, 811-825, 2019.  
549 Faria, S. H., Kipfstuhl, S., Lambrecht, A., Faria, S. H., Kipfstuhl, S., and Lambrecht, A.: EPICA-DML Deep Ice Core:  
550 A Visual Record. In: *Epica-Dml Deep Ice Core: A Visual Record*, *Frontiers in Earth Sciences*, 2018.  
551 Fudge, T. J., et al.: Onset of deglacial warming in West Antarctica driven by local orbital forcing, *Nature*, 500,  
552 440-444, 2013.  
553 Fujita, S., Parrenin, F., Severi, M., Motoyama, H., and Wolff, E. W.: Volcanic synchronization of Dome Fuji and  
554 Dome C Antarctic deep ice cores over the past 216 kyr, *Clim. Past.*, 11, 1395-1416, 2015.  
555 Gautier, E., Savarino, J., Erbland, J., Lanciki, A., and Possenti, P.: Variability of sulfate signal in ice core records  
556 based on five replicate cores, *Clim. Past.*, 12, 103-113, 2016.  
557 Gautier, E., et al.: 2600-years of stratospheric volcanism through sulfate isotopes, *Nature Communications*, 10,  
558 2019.  
559 Gkinis, V., Simonsen, S. B., Buchardt, S. L., White, J. W. C., and Vinther, B. M.: Water isotope diffusion rates  
560 from the NorthGRIP ice core for the last 16,000 years - Glaciological and paleoclimatic implications, *Earth*  
561 *Planet. Sci. Lett.*, 405, 132-141, 2014.  
562 Graf, H. F. and Timmreck, C.: A general climate model simulation of the aerosol radiative effects of the Laacher  
563 See eruption (10,900 B.C.), *Journal of Geophysical Research Atmospheres*, 106, 14747-14756, 2001.  
564 Hammer, C. U., Clausen, H. B., and Dansgaard, W.: Greenland ice sheet evidence of post-glacial volcanism and  
565 its climatic impact, *Nature*, 288, 230-235, 1980.  
566 Holliday, V. T., Bartlein, P. J., Scott, A. C., and Marlon, J. R.: Extraordinary Biomass-Burning Episode and Impact  
567 Winter Triggered by the Younger Dryas Cosmic Impact ~12,800 Years Ago, Parts 1 and 2: A Discussion,  
568 *The Journal of Geology*, 128, 69-94, 2020.  
569 Johnsen, S. J., Dahl-Jensen, D., Gundestrup, N., Steffensen, J. P., Clausen, H. B., Miller, H., Masson-Delmotte, V.,  
570 Sveinbjornsdottir, A. E., and White, J.: Oxygen isotope and palaeotemperature records from six  
571 Greenland ice-core stations: Camp Century, Dye-3, GRIP, GISP2, Renland and NorthGRIP, *J. Quat. Sci.*, 16,  
572 299-307, 2001.  
573 Kawamura, K., et al.: Northern Hemisphere forcing of climatic cycles in Antarctica over the past 360,000 years,  
574 *Nature*, 448, 912-U914, 2007.  
575 Kennett, J. P., et al.: Bayesian chronological analyses consistent with synchronous age of 12,835-12,735 Cal B.P.  
576 for Younger Dryas boundary on four continents, *Proc. Natl. Acad. Sci. U. S. A.*, 112, E4344-E4353, 2015.  
577 Kindler, P., Guillevic, M., Baumgartner, M., Schwander, J., Landais, A., and Leuenberger, M.: Temperature  
578 reconstruction from 10 to 120 kyr b2k from the NGRIP ice core, *Clim. Past.*, 10, 887-902, 2014.  
579 Kjær, K. H., et al.: A large impact crater beneath Hiawatha Glacier in northwest Greenland, *Science Advances*, 4,  
580 2018.  
581 Koffman, B. G., Kreutz, K. J., Kurbatov, A. V., and Dunbar, N. W.: Impact of known local and tropical volcanic  
582 eruptions of the past millennium on the WAIS Divide microparticle record, *Geophysical Research Letters*,  
583 40, 4712-4716, 2013.  
584 Kopec, B. G., Feng, X., Posmentier, E. S., and Sonder, L. J.: Seasonal Deuterium Excess Variations of Precipitation  
585 at Summit, Greenland, and their Climatological Significance, *Journal of Geophysical Research:*  
586 *Atmospheres*, 124, 72-91, 2019.  
587 Kostov, Y., Marshall, J., Hausmann, U., Armour, K. C., Ferreira, D., and Holland, M. M.: Fast and slow responses  
588 of Southern Ocean sea surface temperature to SAM in coupled climate models, *Climate Dynamics*, 48,  
589 1595-1609, 2017.



- 590 Landais, A., et al.: A review of the bipolar see-saw from synchronized and high resolution ice core water stable  
591 isotope records from Greenland and East Antarctica, *Quaternary Science Reviews*, 114, 18-32, 2015.
- 592 Lane, C. S., Blockley, S. P. E., Mangerud, J., Smith, V. C., Lohne, Ø., Tomlinson, E. L., Matthews, I. P., and Lotter,  
593 A. F.: Was the 12.1ka Icelandic Vedde Ash one of a kind?, *Quaternary Science Reviews*, 33, 87-99, 2012.
- 594 Lavigne, F., et al.: Source of the great A.D. 1257 mystery eruption unveiled, Samalas volcano, Rinjani Volcanic  
595 Complex, Indonesia, *Proc. Natl. Acad. Sci. U. S. A.*, 110, 16742-16747, 2013.
- 596 Lee, S. Y., Chiang, J. C. H., Matsumoto, K., and Tokos, K. S.: Southern Ocean wind response to North Atlantic  
597 cooling and the rise in atmospheric CO<sub>2</sub>: Modeling perspective and paleoceanographic implications,  
598 *Paleoceanography*, 26, 2011.
- 599 Lemieux-Dudon, B., Blayo, E., Petit, J. R., Waelbroeck, C., Svensson, A., Ritz, C., Barnola, J. M., Narcisi, B. M., and  
600 Parrenin, F.: Consistent dating for Antarctic and Greenland ice cores, *Quaternary Science Reviews*, 29, 8-  
601 20, 2010.
- 602 Markle, B. R., et al.: Global atmospheric teleconnections during Dansgaard-Oeschger events, *Nature*  
603 *Geoscience*, 10, 36-40, 2017.
- 604 Marshall, G. J. and Thompson, D. W. J.: The signatures of large-scale patterns of atmospheric variability in  
605 Antarctic surface temperatures, *Journal of Geophysical Research*, 121, 3276-3289, 2016.
- 606 Masson-Delmotte, V., et al.: Abrupt change of antarctic moisture origin at the end of termination II, *Proc. Natl.*  
607 *Acad. Sci. U. S. A.*, 107, 12091-12094, 2010.
- 608 Mayewski, P. A., Meeker, L. D., Twickler, M. S., Whitlow, S., Yang, Q. Z., Lyons, W. B., and Prentice, M.: Major  
609 features and forcing of high-latitude northern hemisphere atmospheric circulation using a 110,000-year-  
610 long glaciochemical series, *Journal of Geophysical Research-Oceans*, 102, 26345-26366, 1997.
- 611 Mekhaldi, F., et al.: Multiradionuclide evidence for the solar origin of the cosmic-ray events of 774/5 and  
612 993/4, *Nature Communications*, 6, 2015.
- 613 Moore, C. R., et al.: Widespread platinum anomaly documented at the Younger Dryas onset in North American  
614 sedimentary sequences, *Scientific Reports*, 7, 2017.
- 615 Moore, J. C., Mulvaney, R., and Paren, J. G.: Dielectric stratigraphy of ice: A new technique for determining  
616 total ionic concentrations in polar ice cores, *Geophysical Research Letters*, 16, 1177-1180, 1989.
- 617 Mortensen, A. K., Bigler, M., Grönvold, K., Steffensen, J. P., and Johnsen, S. J.: Volcanic ash layers from the Last  
618 Glacial Termination in the NGRIP ice core, *J. Quat. Sci.*, 20, 209-219, 2005.
- 619 Muscheler, R., Adolphi, F., Heaton, T. J., Ramsey, C. B., Svensson, A., Plicht, J. v. d., and Reimer, P. J.: Testing  
620 and improving the IntCal20 calibration curve with independent records, *Radiocarbon*, In review,  
621 February 2020. In review, February 2020.
- 622 Narcisi, B., Petit, J. R., and Langone, A.: Last glacial tephra layers in the Talos Dome ice core (peripheral East  
623 Antarctic Plateau), with implications for chronostratigraphic correlations and regional volcanic history,  
624 *Quaternary Science Reviews*, 165, 111-126, 2017.
- 625 North Greenland Ice Core Project members: High-resolution record of Northern Hemisphere climate extending  
626 into the last interglacial period, *Nature*, 431, 147-151, 2004.
- 627 Palais, J. M., Germani, M. S., and Zielinski, G. A.: Inter-hemispheric transport of volcanic ash from a 1259 AD  
628 volcanic eruption to the Greenland and Antarctic ice sheets, *Geophysical Research Letters*, 19, 801-804,  
629 1992.
- 630 Pang, H., et al.: Influence of Summer Sublimation on  $\delta D$ ,  $\delta^{18}O$ , and  $\delta^{17}O$  in Precipitation, East Antarctica, and  
631 Implications for Climate Reconstruction From Ice Cores, *Journal of Geophysical Research: Atmospheres*,  
632 124, 7339-7358, 2019.
- 633 Pedro, J. B., Jochum, M., Buizert, C., He, F., Barker, S., and Rasmussen, S. O.: Beyond the bipolar seesaw:  
634 Toward a process understanding of interhemispheric coupling, *Quaternary Science Reviews*, 192, 27-46,  
635 2018.



- 636 Petaev, M. I., Huang, S., Jacobsen, S. B., and Zindler, A.: Large Pt anomaly in the Greenland ice core points to a  
637 cataclysm at the onset of Younger Dryas, *Proc. Natl. Acad. Sci. U. S. A.*, 110, 12917-12920, 2013.
- 638 Raisbeck, G. M., et al.: An improved north-south synchronization of ice core records around the 41 kyr Be-10  
639 peak, *Clim. Past.*, 13, 217-229, 2017.
- 640 Raisbeck, G. M., Yiou, F., Jouzel, J., and Stocker, T. F.: Direct north-south synchronization of abrupt climate  
641 change records in ice cores using beryllium 10, *Clim. Past.*, 3, 541–547, 2007.
- 642 Rasmussen, S. O., et al.: A first chronology for the north greenland eemian ice drilling (NEEM) ice core, *Clim.*  
643 *Past.*, 9, 2713-2730, 2013.
- 644 Rasmussen, S. O., et al.: A new Greenland ice core chronology for the last glacial termination, *Journal of*  
645 *Geophysical Research*, 111, D06102, doi:06110.01029/02005JD006079, 2006.
- 646 Rasmussen, S. O., et al.: A stratigraphic framework for abrupt climatic changes during the Last Glacial period  
647 based on three synchronized Greenland ice-core records: Refining and extending the INTIMATE event  
648 stratigraphy, *Quaternary Science Reviews*, 106, 14-28, 2014.
- 649 Ruth, U., et al.: Proxies and measurement techniques for mineral dust in antarctic ice cores, *Environmental*  
650 *Science and Technology*, 42, 5675-5681, 2008.
- 651 Ruth, U., et al.: "EDML1": a chronology for the EPICA deep ice core from Dronning Maud Land, Antarctica, over  
652 the last 150 000 years, *Clim. Past.*, 3, 475-484, 2007.
- 653 Ruth, U., Wagenbach, D., Steffensen, J. P., and Bigler, M.: Continuous record of microparticle concentration and  
654 size distribution in the central Greenland NGRIP ice core during the last glacial period, *Journal of*  
655 *Geophysical Research*, 108, 4098, doi:4010.1029/2002JD002376, 2003.
- 656 Schmidt, G. A., LeGrande, A. N., and Hoffmann, G.: Water isotope expressions of intrinsic and forced variability  
657 in a coupled ocean-atmosphere model, *Journal of Geophysical Research-Atmospheres*, 112, 2007.
- 658 Schwander, J. and Stauffer, B.: Age difference between polar ice and the air trapped in its bubbles, *Nature*, 311,  
659 45-47, 1984.
- 660 Schüpbach, S., et al.: Greenland records of aerosol source and atmospheric lifetime changes from the Eemian  
661 to the Holocene, *Nature Communications*, 9, 2018.
- 662 Seierstad, I. K., et al.: Consistently dated records from the Greenland GRIP, GISP2 and NGRIP ice cores for the  
663 past 104 ka reveal regional millennial-scale delta O-18 gradients with possible Heinrich event imprint,  
664 *Quaternary Science Reviews*, 106, 29-46, 2014.
- 665 Severi, M., et al.: Synchronisation of the EDML and EDC ice cores for the last 52 kyr by volcanic signature  
666 matching, *Clim. Past.*, 3, 367-374, 2007.
- 667 Severi, M., Udisti, R., Becagli, S., Stenni, B., and Traversi, R.: Volcanic synchronisation of the EPICA-DC and  
668 TALDICE ice cores for the last 42 kyr BP, *Clim. Past.*, 8, 509-517, 2012.
- 669 Sigl, M., et al.: The WAIS Divide deep ice core WD2014 chronology - Part 2: Annual-layer counting (0-31 ka BP),  
670 *Clim. Past.*, 12, 769-786, 2016.
- 671 Sigl, M., et al.: A new bipolar ice core record of volcanism from WAIS Divide and NEEM and implications for  
672 climate forcing of the last 2000 years, *Journal of Geophysical Research Atmospheres*, 118, 1151-1169,  
673 2013.
- 674 Sigl, M., et al.: Timing and climate forcing of volcanic eruptions for the past 2,500 years, *Nature*, 523, 543-+,  
675 2015.
- 676 Steffensen, J. P., et al.: High-resolution Greenland ice core data show abrupt climate change happens in few  
677 years, *Science*, 321, 680-684, 2008.
- 678 Steinhilber, F., et al.: 9,400 years of cosmic radiation and solar activity from ice cores and tree rings, *Proc. Natl.*  
679 *Acad. Sci. U. S. A.*, 109, 5967-5971, 2012.
- 680 Stenni, B., et al.: Expression of the bipolar see-saw in Antarctic climate records during the last deglaciation,  
681 *Nature Geoscience*, 4, 46-49, 2010.



- 682 Stocker, T. F. and Johnsen, S. J.: A minimum thermodynamic model for the bipolar seesaw, *Paleoceanography*,  
683 18, 1087, doi:10.1029/2003PA000920, 2003.
- 684 Stuiver, M. and Grootes, P. M.: GISP2 oxygen isotope ratios, *Quaternary Research*, 53, 277-284, 2000.
- 685 Svensson, A., et al.: A 60 000 year Greenland stratigraphic ice core chronology, *Clim. Past.*, 4, 47-57, 2008.
- 686 Svensson, A., et al.: Direct linking of Greenland and Antarctic ice cores at the Toba eruption (74 ka BP), *Clim.*  
687 *Past.*, 9, 749-766, 2013.
- 688 Svensson, A., Nielsen, S. W., Kipfstuhl, S., Johnsen, S. J., Steffensen, J. P., Bigler, M., Ruth, U., and Röthlisberger,  
689 R.: Visual stratigraphy of the North Greenland Ice Core Project (NorthGRIP) ice core during the last glacial  
690 period, *Journal of Geophysical Research*, 110, D02108, doi:02110.01029/02004JD005134, 2005.
- 691 Uemura, R., Masson-Delmotte, V., Jouzel, J., Landais, A., Motoyama, H., and Stenni, B.: Ranges of moisture-  
692 source temperature estimated from Antarctic ice cores stable isotope records over glacial-interglacial  
693 cycles, *Clim. Past.*, 8, 1109-1125, 2012.
- 694 Veres, D., et al.: The Antarctic ice core chronology (AICC2012): An optimized multi-parameter and multi-site  
695 dating approach for the last 120 thousand years, *Clim. Past.*, 9, 1733-1748, 2013.
- 696 Vettoretti, G. and Peltier, W. R.: Interhemispheric air temperature phase relationships in the nonlinear  
697 Dansgaard-Oeschger oscillation, *Geophysical Research Letters*, 42, 1180-1189, 2015.
- 698 Voelker, A. H. L. and workshop participants: Global distribution of centennial-scale records for Marine Isotope  
699 Stage (MIS) 3: A database, *Quaternary Science Reviews*, 21, 1185-1212, 2002.
- 700 Wegner, A., Fischer, H., Delmonte, B., Petit, J. R., Erhardt, T., Ruth, U., Svensson, A., Vinther, B., and Miller, H.:  
701 The role of seasonality of mineral dust concentration and size on glacial/interglacial dust changes in the  
702 EPICA Dronning Maud Land ice core, *Journal of Geophysical Research-Atmospheres*, 120, 2015.
- 703 Wilhelms, F., Kipfstuhl, J., Miller, H., Heinloth, K., and Firestone, J.: Precise dielectric profiling of ice cores: A  
704 new devise with improved guarding and its theory, *J. Glaciol.*, 44, 171-174, 1998.
- 705 Winter, A., Steinhage, D., Creyts, T. T., Kleiner, T., and Eisen, O.: Age stratigraphy in the East Antarctic Ice Sheet  
706 inferred from radio-echo sounding horizons, *Earth System Science Data*, 11, 1069-1081, 2019.
- 707 Wolff, E. W., Moore, J. C., Clausen, H. B., and Hammer, C. U.: Climatic implications of background acidity and  
708 other chemistry derived from electrical studies of the Greenland Ice Core Project ice core, *Journal of*  
709 *Geophysical Research*, 102, 26325-26332, 1997.
- 710 Zielinski, G. A., Mayewski, P. A., Meeker, D., Grönvold, K., Germani, M. S., Whitlow, S., Twickler, M. S., and  
711 Taylor, K.: Volcanic aerosol records and tephrochronology of the Summit, Greenland, ice cores, *Journal of*  
712 *Geophysical Research*, 102, 26625-26640, 1997.
- 713
- 714



715 Table 1.

Period	NGRIP depth(m)	NEEM depth(m)	GRIP depth(m)	GISP2 depth(m)	EDML depth(m)	EDC depth(m)	WDC depth(m)	GICC05 age(b2k)	WD2014 age(b2k)	Comments
GS-1	1506.11	1429.08	1639.53	1692.25	700.18	370.09	2012.50	12170	12113	Vedde ash
	1508.05	1430.56	1641.68	1694.24	703.40	371.94	2019.07	12241	12186	
	1522.20	1441.43	1657.52	1708.64	725.83	384.13	2068.41	12755	12740	
GI-1	1527.31	1445.01	1663.33	1713.92	731.46	387.28	2082.95	12917	12897	Onset YD 4 spikes
	1529.05	1446.09	1665.26	1715.71	732.63	388.03	2086.53	12961	12933	Onset YD 4 spikes
	1530.49	1447.06	1667.00	1717.29	733.68	388.71	2089.55	12995	12965	Onset YD 4 spikes
	1531.78	1447.94	1668.48	1718.67	734.77	389.36	2092.72	13028	12998	Onset YD 4 spikes
	1538.35	1452.02	1676.25	1725.74	741.24	393.01	2111.25	13212	13185	
	1555.52	1462.37	1696.15	1744.25	754.71	400.28	2145.41	13620	13559	
	1595.04	1484.04	1742.28	1787.32	784.90	417.01	2219.81	14500	14404	
GS-2.1	1605.00	1489.47	1753.75	1798.17	793.21	421.88	2240.15	14705	14632	
	1606.52	1490.35	1755.46	1799.77	795.52	423.06	2245.21	14761	14688	
	1611.97	1493.30	1761.44	1805.39	803.86	427.11	2263.20	14966	14899	
	1619.54	1497.56	1769.48	1812.80	817.26	433.78	2290.21	15296	15234	
	1625.57		1775.82	1818.88	826.00	438.10	2308.70	15559	15466	
	1645.85		1796.72	1838.60	859.70	454.00	2370.00	16469	16455	
LGM										
GS-3	1814.92	1610.35	1973.03	2006.76	1051.82	553.36	2634.35	24669	24589	Triplet
	1827.21	1617.11			1069.72	561.38	2660.24	25460	25366	
	1831.58	1619.60		2022.74	1076.94	564.43	2670.09	25759	25671	
	1834.25	1621.00			1080.83	566.21	2675.70	25940	25847	
GI-3/GS-4	1869.52	1641.23	2025.8	2057.05	1123.98	586.28	2742.86	27797	27833	
	1880.00	1647.55	2035.3	2066.17	1138.00	593.49	2768.10	28454	28534	
GS-5.1	1892.34				1146.80	598.87	2784.36	28942	29028	
	1902.84		2056.0	2086.38	1160.15	607.05	2806.62	29678	29721	
	1903.45	1661.59			1160.95			29722		
	1910.97	1665.98		2092.92	1170.18	613.20	2822.20	30244	30255	
GI-5.2/GS-5.2	1939.54	1683.32	2087.8	2117.06	1199.60	632.28	2863.15	32032	N/A	
	1949.59	1688.83	2096.9	2125.72	1206.06	636.42	2872.32	32433	N/A	
GS-6	1962.24	1696.24			1220.12	644.78	2890.77	33221	N/A	
	1963.75			2137.48	1222.02	645.86	2893.14	33328	N/A	Doublet
GS-7	1982.33				1239.19	656.37	2915.12	34227	N/A	
GI-7/GS-7	1989.90	1712.05	2131.40	2160.07	1248.00	661.85	2928.33	34718	N/A	
	2000.22	1717.88	2140.49	2169.35	1254.95	666.34	2939.57	35145	N/A	
GS-8/GI-7	2010.98	1724.05	2150.00	2179.13	1262.29	671.08	2951.03	35556	N/A	



GI-8	2038.07	1740.25	2172.15	2202.73	1291.80	689.12	2987.25	37113	N/A
	2042.28	1742.65	2175.90	2206.65	1295.11	691.15	2991.13	37277	N/A
	2061.99	1754.19	2193.33	2224.84	1307.60	699.08	3006.32	37965	N/A
GS-9	2067.36	1757.30	2197.99	2229.71	1311.08	701.26	3010.47	38133	N/A
	2070.24		2200.51	2232.37	1313.08	702.59	3012.89	38232	N/A
	2072.48	1760.39		2234.14	1316.04	704.16	3016.48	38366	N/A
	2094.13	1774.31			1349.53	723.19	3052.10	39869	N/A
GS-10	2094.88	1774.76		2252.11	1350.56	723.84	3053.26	39915	N/A
	2100.03	1777.73	2223.93	2256.31	1354.57	726.31	3057.95	40183	N/A
	<b>2106.01</b>				<b>1362.28</b>	<b>730.95</b>		40563	N/A BeA
	<b>2109.62</b>				<b>1366.56</b>	<b>733.85</b>		40794	N/A BeB
GS-11	<b>2113.22</b>				<b>1370.57</b>	<b>736.27</b>		41002	N/A BeC
	2116.18	1786.94	2236.82	2269.63	1372.72	737.50	3079.07	41144	N/A
	2121.86	1790.01	2241.56	2274.58	1376.92		3083.95	41379	N/A
	<b>2129.82</b>				<b>1386.61</b>	<b>745.98</b>		41858	N/A BeD
GS-12	2130.21				1387.31	746.42	3095.68	41887	N/A
	2132.21	1796.08			1390.02	748.08	3098.61	42037	N/A
	<b>2132.64</b>				<b>1390.49</b>	<b>748.47</b>		42067	N/A BeE
	2133.28		2250.55		1391.45	748.96	3100.16	42111	N/A
GS-13	2135.13	1797.95	2252.05	2285.24	1393.78	750.33	3102.68	42250	N/A
	2142.36	1801.80	2257.93	2291.16	1400.14	754.37	3109.97	42658	N/A
	2151.80	1807.00	2265.98	2299.22	1408.04	759.53	3118.82	43104	N/A
	2157.20	1809.94	2270.52	2303.70	1411.97	762.24	3123.40	43327	N/A
GI-12	2173.90	1819.87	2283.64	2317.11	1431.27	775.02	3144.96	44507	N/A
	2182.77	1824.74	2291.05	2324.64	1439.07	780.58	3154.24	45050	N/A
	<b>2191.97</b>	<b>1829.66</b>	<b>2298.74</b>	<b>2332.68</b>	<b>1446.26</b>	<b>785.97</b>	<b>3162.93</b>	45555	N/A
	2201.55	1834.82	2306.90	2341.17	1452.62	790.58	3170.99	46002	N/A
GS-14	2204.14	1836.23	2309.13	2343.48	1454.36	791.88	3173.19	46116	N/A
	2217.64	1843.68	2320.51	2355.20	1462.99	798.50	3184.42	46683	N/A
	2224.62	1848.15		2360.97	1468.91	802.87	3192.00	47023	N/A
	2227.22		2328.03	2362.94	1472.47	805.18	3196.10	47214	N/A
GS-15.1	2242.20		2339.03	2374.00	1494.11	819.25	3218.78	48441	N/A
	2252.88	1863.15	2347.35	2382.30	1503.60	826.00	3228.32	49065	N/A
	2257.55	1865.65	2351.03	2386.05	1507.33	828.55	3231.90	49319	N/A
	2277.65	1876.39	2366.64	2401.80	1526.13	841.62	3249.64	50586	N/A
GS-15.2	2302.75	1889.52	2386.63	2421.67	1547.79	856.76	3271.39	52031	N/A
	2307.61	1892.00	2390.60	2425.62	1551.53	859.49	3274.77	52302	N/A
	2326.10	1901.77	2405.45	2440.00	1568.29	871.41	3289.90	53259	N/A
	2344.59	1911.42	2420.10	2454.19	1583.34	882.27	3306.60	54178	N/A
GS-15.1	2347.73				1587.05	884.80	3309.90	54390	N/A
GS-15.2	2355.40				1596.69	891.34	3317.95	55005	N/A



	2359.45	1919.82	2431.00	2464.26	1602.80	895.60	3322.15	55383	N/A	NAAZ II
<b>GI-16.1</b>	2382.65		2447.88	2480.28	1628.50	914.18	3338.62	57051	N/A	
	2385.25	1933.39	2449.79	2482.04	1630.90		3340.35	57222	N/A	
	2389.49		2453.11	2485.05	1635.13	919.15	3343.00	57499	N/A	
<b>GI-16.2</b>	2400.69	1941.27	2461.59	2493.25	1645.95	927.11	3348.89	58182	N/A	
	2403.59				1648.91	929.20	3350.32	58355	N/A	
	2416.26				1662.73	939.54	3357.90	59180	N/A	
<b>GI-17.2</b>	2417.90				1665.24	941.30	3359.30	59317	N/A	
<b>GS-18</b>	2421.72			2507.702	1670.14	944.59	3361.90	59545	N/A	
	2422.82				1672.31	946.10	3362.95	59647	N/A	

716

717



718 Table 2a.

GI-event	Greenland interstadial onset depth (m)							GICC05 age (yr b2k)	Distance (yr)	Uncertainty (yr)
	NGRIP	NEEM	GRIP	GISP2	EDML	EDC	WDC			
YD-PB	1490.89	1418.75	1622.08	1675.61	676.46	356.32	1962.70	11669	-20	2
1	1604.64	1489.26	1753.34	1797.78	792.70	421.58	2238.95	14693	-13	1
3	1869.00	1640.94	2025.32	2056.57	1123.54	586.08	2742.16	27776	-20	2
4	1891.27	1654.11	2045.81	2076.33	1145.97	598.37	2782.83	28888	-51	5
5.1	1919.48	1671.51	2070.21	2099.96	1179.08	619.07	2835.50	30781	498	50
5.2	1951.66	1690.04	2098.82	2127.52	1207.26	637.16	2874.01	32500	68	7
6	1974.48	1703.17	2118.52	2147.03	1229.98	650.73	2903.17	33737	409	41
7	2009.62	1723.26	2148.80	2177.90	1260.99	670.24	2949.01	35487	-71	7
8	2069.88	1758.82	2200.19	2232.03	1312.67	702.32	3012.40	38215	-20	2
9	2099.50	1777.43	2223.52	2255.87	1354.20	726.08	3057.51	40154	-24	2
10	2123.98	1791.21	2243.22	2276.30	1378.51	741.14	3085.75	41457	83	8
11	2157.58	1810.16	2270.82	2304.00	1412.29	762.45	3123.76	43346	18	2
12	2221.96	1846.28	2323.98	2358.79	1465.79	800.57	3188.00	46843	-177	18
13	2256.73	1865.21	2350.38	2385.39	1506.61	828.05	3231.20	49271	-48	5
14	2345.39	1911.86	2420.68	2454.73	1583.95	882.69	3307.14	54213	36	4
15.1	2355.17	1917.40	2427.86	2461.37	1596.44	891.17	3317.75	54990	-15	2
15.2	2366.15	1923.24	2435.93	2469.02	1609.21	900.36	3326.36	55787	406	41
16.1	2398.71	1940.25	2460.18	2491.91	1643.43	925.25	3347.52	58037	-152	15
16.2	2402.25	1942.05	2462.74	2494.33	1647.22	928.01	3349.52	58258	-103	10
17.1	2414.82	1948.37	2472.05	2503.02	1660.55	937.91	3356.71	59067	-125	12
17.2	2420.35	1951.08	2476.15	2506.86	1667.53	942.84	3360.52	59435	-132	13

719

720



721 Table 2b.

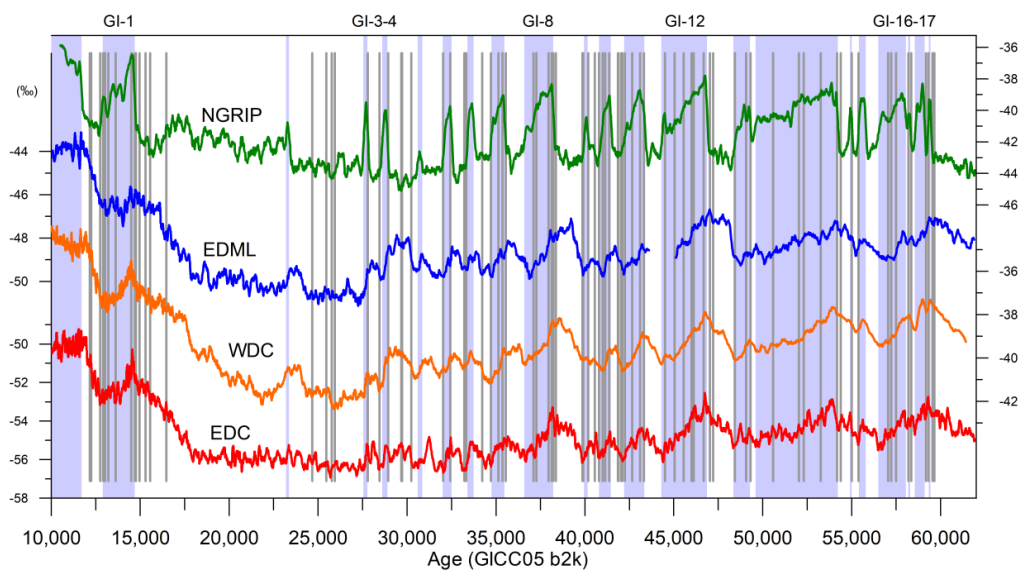
GI-event	Greenland interstadial termination depth (m)							GICC05 age (yr b2k)	Distance (yr)	Uncertainty (yr)
	NGRIP	NEEM	GRIP	GISP2	EDML	EDC	WDC			
BA-YD	1524.21	1442.83	1659.79	1710.70	728.33	385.53	2074.86	12826	70	7
3	1861.91	1636.91	2018.50	2050.17	1118.41	583.69	2733.94	27548	-247	25
4	1882.59	1649.04	2037.69	2068.53	1140.75	595.17	2773.18	28599	144	14
5.1	1916.45	1669.74	2067.61	2097.44	1176.51	617.40	2831.89	30621	354	35
5.2	1939.71	1683.41	2087.98	2117.21	1199.75	632.37	2863.36	32042	9	1
6	1964.52	1697.55	2109.93	2138.17	1223.04	646.48	2894.41	33374	47	5
7	1990.58	1712.44	2132.00	2160.68	1248.60	662.24	2929.30	34753	36	4
8	2027.43	1733.94	2163.25	2193.23	1282.58	683.27	2976.19	36620	-504	50
9	2095.51	1775.13	2220.41	2252.62	1351.26	724.27	3054.08	39955	40	4
10	2112.53	1784.96	2233.80	2266.44	1369.94	735.89	3075.84	40968	-39	4
11	2135.66	1798.19	2252.48	2285.68	1394.25	750.63	3103.22	42281	31	3
12	2171.17	1818.25	2281.50	2314.92	1429.09	773.57	3142.52	44358	-144	14
13	2242.85	1857.83	2339.54	2374.51	1494.80	819.77	3219.51	48490	48	5
14	2261.49	1867.76	2354.09	2389.14	1511.69	831.58	3236.02	49602	282	28
15.1	2353.66	1916.55	2426.76	2460.35	1595.02	890.21	3316.61	54901	-101	10
15.2	2359.92	1920.06	2431.35	2464.59	1603.35	896.01	3322.51	55419	35	4
16.1	2375.88	1928.41	2442.94	2475.66	1621.92	908.87	3333.90	56605	-444	44
16.2	2400.56	1941.21	2461.50	2493.16	1645.82	927.02	3348.82	58174	-8	1
17.1	2406.52	1944.20	2465.91	2497.28	1652.67	932.01	3352.41	58594	243	24
17.2	2417.77	1949.85	2474.23	2505.06	1665.07	941.18	3359.21	59307	-9	1

722

723



724 **Figure 1:**

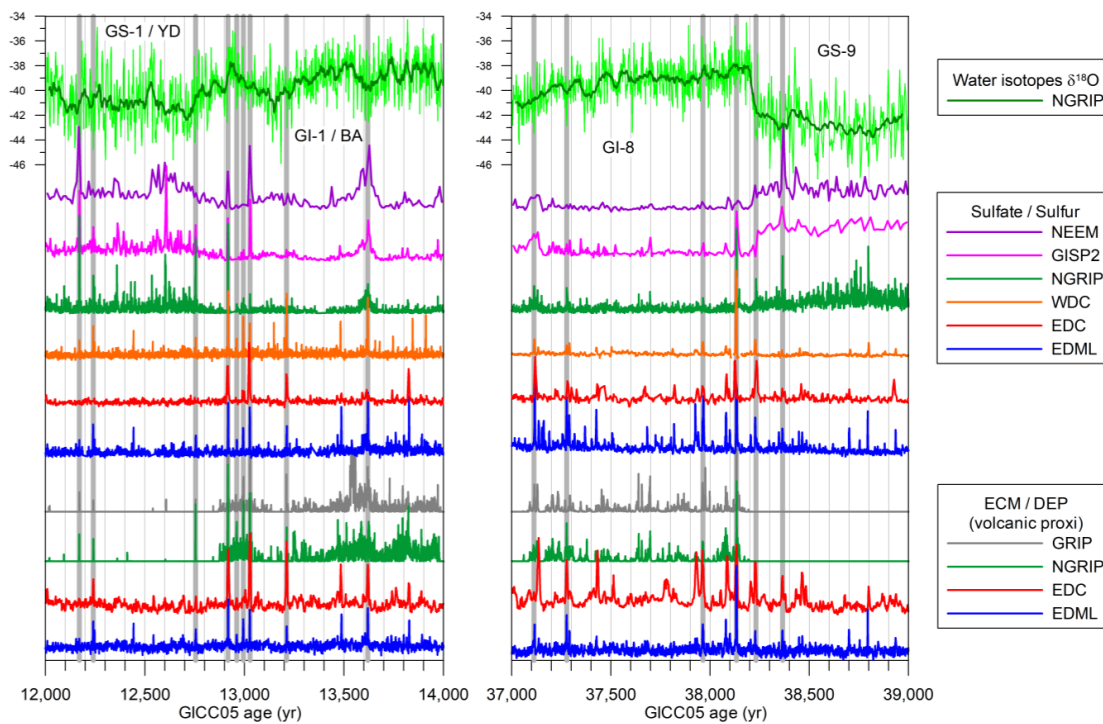


725

726

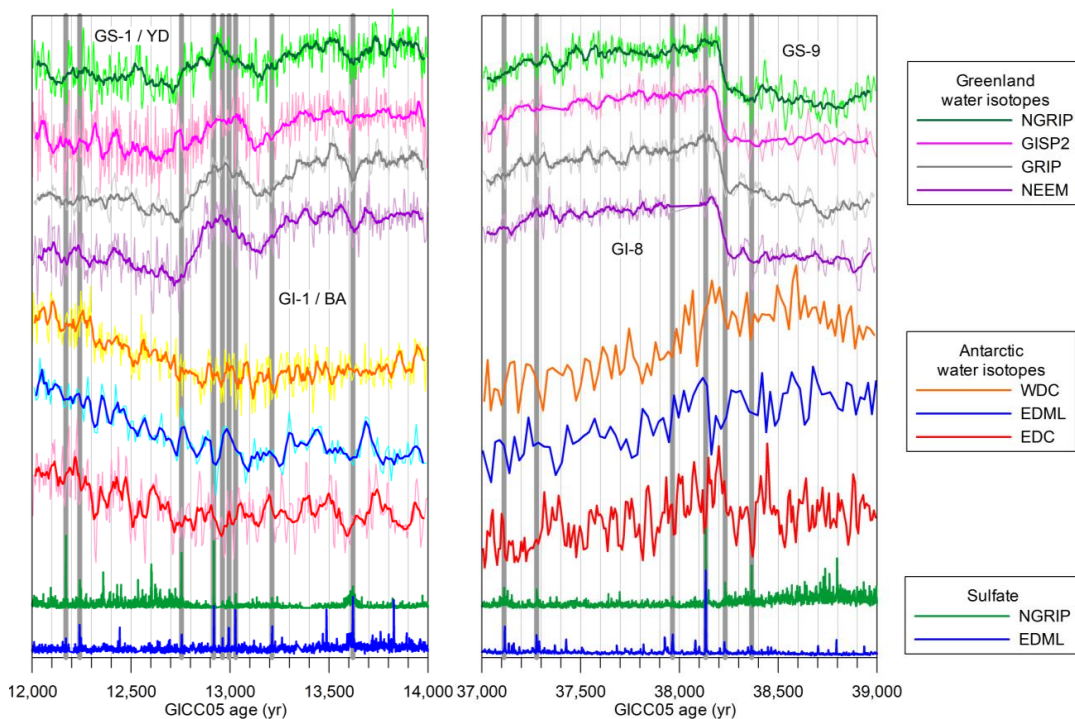


727 **Figure 2:**





730 **Figure 3:**

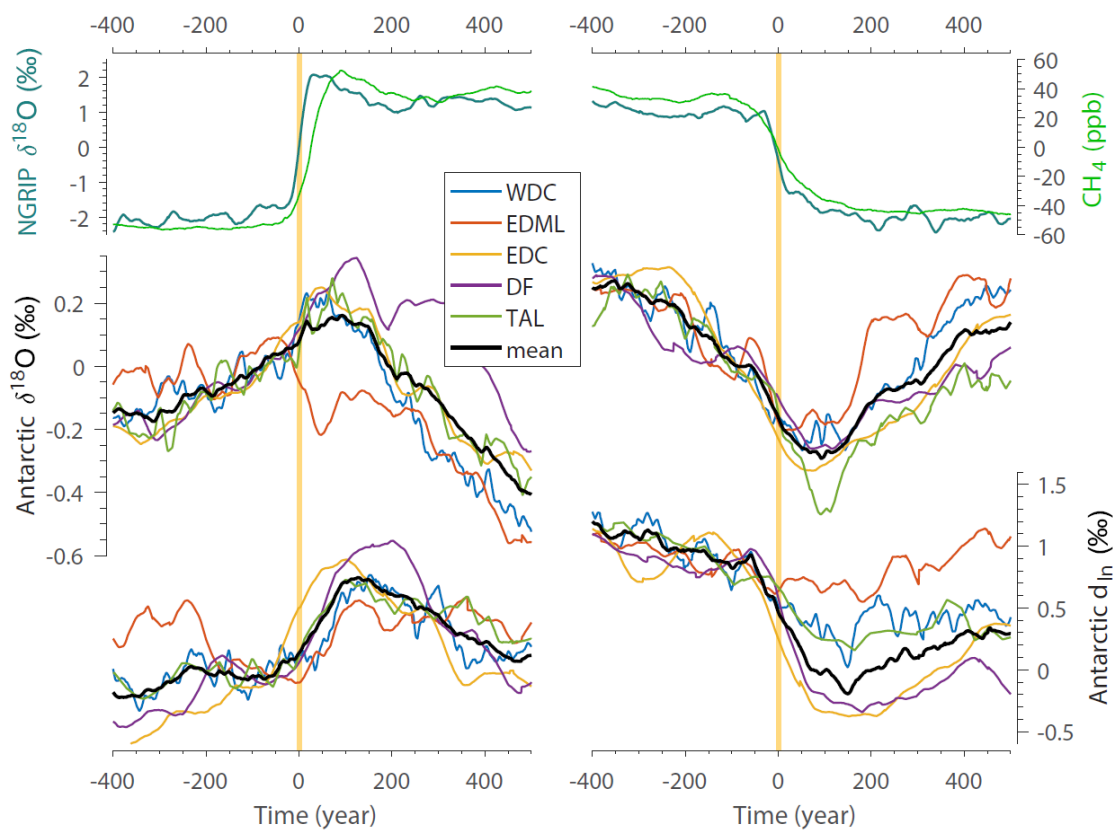


731

732



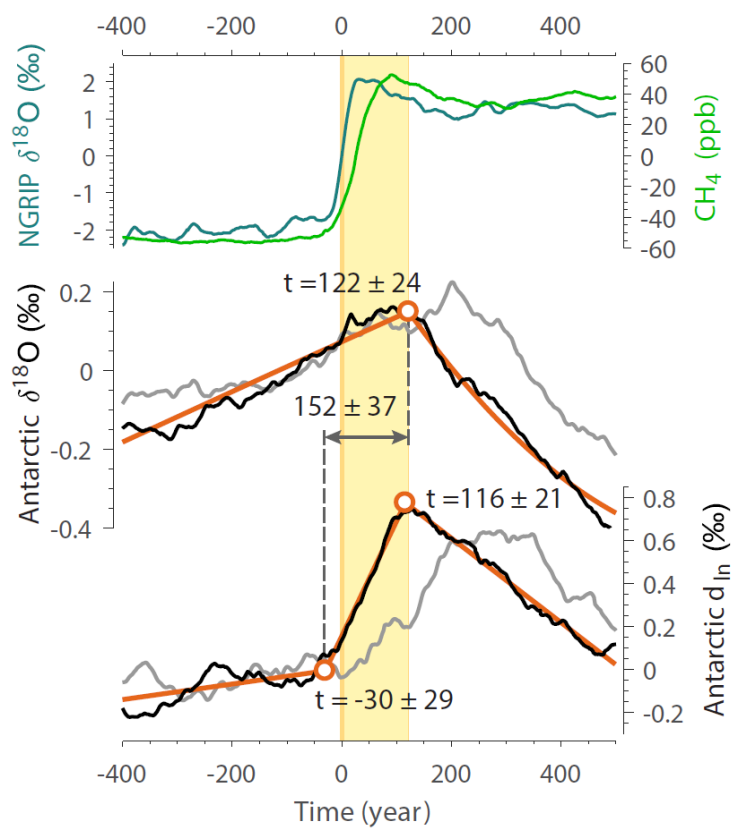
733 **Figure 4:**



734



735 **Figure 5:**



736

737